



Fabrication of Microbicidal Silver Nanoparticles: Green Synthesis and Implications in the Containment of Bacterial Biofilm on Orthodontal Appliances

Saba Farheen^{1†}, Abdul M Oanz^{1†}, Nazoora Khan^{1†}, Mohd Saad Umar¹, Fauzia Jamal¹, Ishrat Altaf¹, Mohammad Kashif², Ansam Wadia Alshameri¹, Satyanarayana Somavarapu³, Irfan Ahmad Wani¹, Saba Khan^{4*} and Mohammad Owais^{1*}

¹Interdisciplinary Biotechnology Unit, Aligarh Muslim University, Aligarh, India, ²CSIR-NBRI, Lucknow, India, ³Department of Pharmaceutics, UCL School of Pharmacy, London, United Kingdom, ⁴Department of Orthodontics, Dental College, Aligarh Muslim University, Aligarh, India

OPEN ACCESS

Edited by:

Pradeep Verma,
Central University of Rajasthan, India

Reviewed by:

Vijayakumar Sekar,
Shandong University, China
Renata Lima,
University of Sorocaba, Brazil

*Correspondence:

Saba Khan
sabakhan.ortho@gmail.com
Mohammad Owais
owais_lakhnawi@yahoo.com

[†]These authors have contributed
equally to this work

Specialty section:

This article was submitted to
Biomedical Nanotechnology,
a section of the journal
Frontiers in Nanotechnology

Received: 21 September 2021

Accepted: 03 March 2022

Published: 07 April 2022

Citation:

Farheen S, Oanz AM, Khan N, Umar MS, Jamal F, Altaf I, Kashif M, Alshameri AW, Somavarapu S, Wani IA, Khan S and Owais M (2022) Fabrication of Microbicidal Silver Nanoparticles: Green Synthesis and Implications in the Containment of Bacterial Biofilm on Orthodontal Appliances. *Front. Nanotechnol.* 4:780783. doi: 10.3389/fnano.2022.780783

Among various metal-based nanoparticles, silver nanoparticles (AgNPs) manifest superior inhibitory effects against several microorganisms. In fact, the AgNP-based treatment has been reported to inhibit both sensitive and resistant isolates of bacteria and other disease-causing microbes with equal propensity. Keeping this fact into consideration, we executed bio-mediated synthesis of AgNPs employing extract of flower and various other parts (such as bud and leaf) of the *Hibiscus rosa-sinensis* plant. The physicochemical characterization of as-synthesized AgNPs was executed employing transmission electron microscopy (TEM), dynamic light scattering (DLS), zeta potential, Fourier transform infrared (FTIR) spectroscopy, and UV-Vis spectroscopy, etc. The as-synthesized AgNPs demonstrated strong antimicrobial activity against both Gram-positive and Gram-negative bacteria with equal propensity. The as-synthesized AgNPs successfully inhibited *Streptococcus mutans* (*S. mutans*), one of the main causative bacteria responsible for dental caries. Considering the fact that orthodontic appliances facilitate infliction of the oral cavity with a range of microbes including *S. mutans*, we determined the growth inhibitory and anti-adherence activities of AgNPs on orthodontic appliances. We performed microbiological assays employing AgNPs adsorbed onto the surface of nickel–titanium (Ni-Ti) orthodontic wires. A topographic analysis of the decontaminated Ni-Ti orthodontic wires was performed by scanning electron microscopy. In addition to antimicrobial and anti-biofilm activities against oral *S. mutans*, the as-fabricated AgNPs demonstrated significant inhibitory and anti-biofilm properties against other biofilm-forming bacteria such as *Escherichia coli* and *Listeria monocytogenes*.

Keywords: silver nanoparticles, biofilm, orthodontic wire, drug resistance, *Streptococcus mutans*

Abbreviations: AgNO₃, silver nitrate; AgNPs, silver nanoparticles; ATCC, American Type Culture Collection; BHI, brain heart infusion; CFU, colony-forming unit; DLS, dynamic light scattering; FTIR, Fourier transform infrared spectroscopy; HRSF, *Hibiscus rosa-sinensis* flower; HRSP, *Hibiscus rosa-sinensis* plant; LB, Luria Bertani; MTCC, microbial type culture collection; NB, nutrient broth; Ni-Ti, nickel–titanium; NP, nanoparticle; ROS, reactive oxygen species; SEM, scanning electron microscopy; TEM, transmission electron microscope.

INTRODUCTION

The nano-sized metal particles exhibit altered chemical and physical attributes compared to their precursor chemical entities. Considering this fact, there has been an increasing propensity in the exploitation of metal-based nanoparticles in diversified fields ranging from optics, catalysis, mechanics, paint industry, to therapeutics and medical diagnostics (Guerrero-Martínez et al., 2010; Abbasi et al., 2016; Khan et al., 2019). Well-dispersed and ultrafine metal nanoparticles acquire distinctive thermodynamic properties when compared to their precursor metal compounds. Because of their nano-order size dimension, high-energy surface atoms, greater penetration potential, and ability to target various vital biological molecules of the host, the nanoparticles have been widely used in various medical science-related fields (Abbasi et al., 2016; Khan et al., 2019).

It is noteworthy that the nanometer size dimension of the particles renders them the ability to traverse various biological barriers of the host body and even guides them to accumulate in tissues either beneath the skin or deeper into the organs like lungs, the liver, and even less accessible components of the central nervous system (CNS) such as the brain (Petros and DeSimone, 2010). As a consequence, the NP-based drug delivery systems have been widely exploited in the treatment of different types of cancer and several infectious diseases (Vashist et al., 2014).

Various chemical and physical methods such as UV or microwave irradiation, chemical reduction, photochemical process, and electron irradiation have been widely employed in the synthesis of nanoparticles (Loo et al., 2012; Iravani et al., 2014; D'Agostino et al., 2016; dos Santos et al., 2019). Incidentally, most of these methods involve multistep processing and high-energy input along with the involvement of hazardous chemicals to carry on the fabrication of nanoparticles. Moreover, the chemical method- and physical method-based NP synthesis entails relatively sophisticated instrumentation and also suffers the shortcomings such as low material conversion and difficulty in purification.

On a positive note, there has been an unanticipated paradigm shift in the exploitation of whole bacteria, fungi, and various parts of the plants (*cf.* leaf, flower, fruit, and etc.) in the synthesis of metal nanoparticles. The “green synthesis” approach has been receiving increased attention as it is environmentally friendly and causes almost negligible pollution of any kind (Bhosale et al., 2014). Furthermore, the cost-effective green synthesis technique has an edge over other methods and can be easily modulated for large-scale production (Ramya and Subapriya, 2012). Moreover, by smart maneuvering of fabrication conditions, the green approach can be manipulated to synthesize nanoparticles with diverse shapes and sizes (Ramya and Subapriya, 2012; Bhosale et al., 2014).

Dental caries, a multifactorial disease, has been considered a serious oral health issue. It is more common in individuals who wear orthodontic appliances. The orthodontic devices not only offer a platform to growing microbes but also pose an obstacle in biofilm removal during oral hygiene procedures. The disease leads to demineralization and erosion of the tooth

enamel surface. Prolonged dental plaque expedites the accumulation of *Streptococcus mutans* (*S. mutans*), the causative oral pathogen, that in turn ensues the development of dental caries (Ritter et al., 2014). Moreover, various orthodontic elastomeric modules, including brackets and wires, when accompanied with poor oral hygiene may lead to the establishment of infection caused by *S. mutans* and several other oral bacteria (Lekhadia, 2018). The bacterial infection is generally accompanied by the formation of biofilm on both tooth enamel and orthodontic appliances used in the dental care setup (Koo et al., 2017). The related oral clinical issues may result in the unacceptable esthetic presentation of the inflicted person. If not treated properly, the infection not only causes bacteremia but also evokes an inflammatory response in the afflicted patients. *S. mutans* infection may also lead to infective endocarditis (Montgomery et al., 2014).

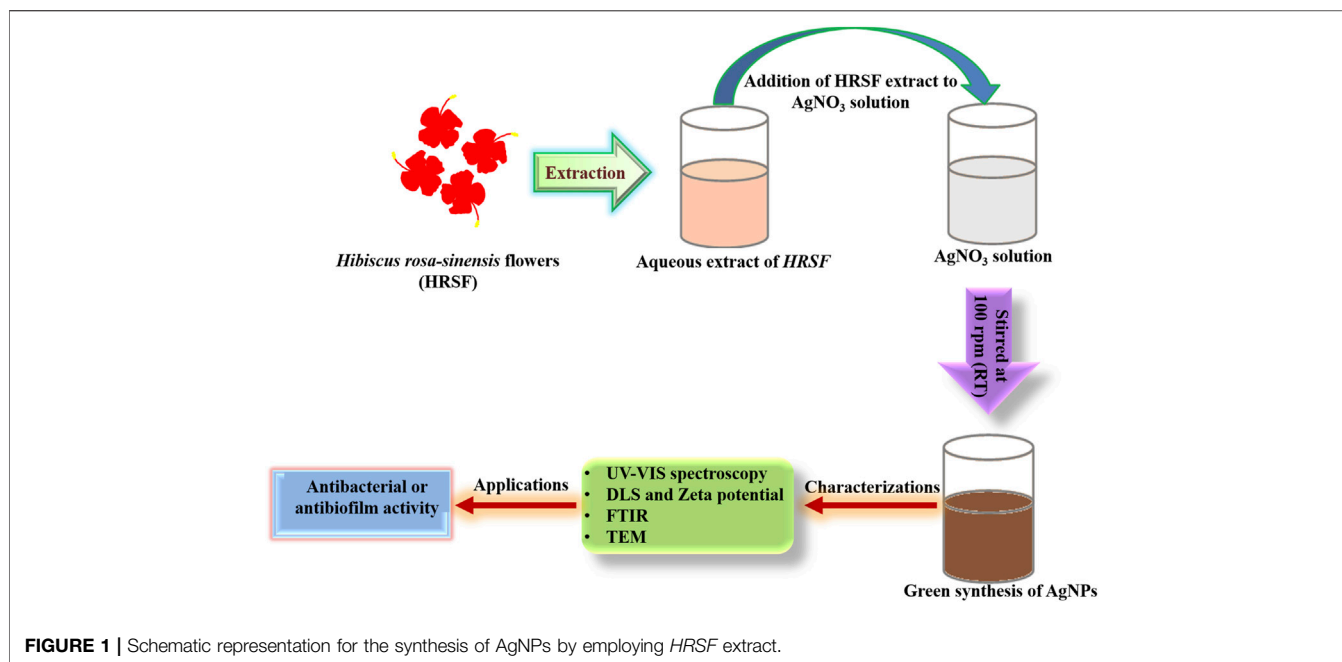
Among various metal-based nanoparticles, silver nanoparticles possess excellent antimicrobial properties against a wide range of microorganisms. The special treatment of orthodontic appliances with AgNPs, before their usage in clinical settings, is likely to combat invading pathogens by manifesting strong anti-biofilm activity (Gallardo et al., 2019).

Hibiscus rosa-sinensis Linn (family Malvaceae) is reported to possess potent medicinal properties including antibacterial, antitumor, cardioprotective, hypotensive, antidiabetic, anticonvulsant, wound healing, and antioxidant activities (Lim, 2014). *Hibiscus rosa-sinensis* (HRS) flowers, buds, and leaves are known to contain flavonoids like anthocyanin and quercetin. The HRSF flavonoids have also been implicated for their antidepressant and anxiolytic activities (Shewale et al., 2012).

In the present study, we first ascertained the potential of extracts of various parts of the *Hibiscus rosa-sinensis* plant (HRSF) to synthesize silver nanoparticles (AgNPs). We found that aqueous extract of different parts of HRSF (flower, bud, and leaf extracts) act as a reducing and capping/stabilizing agent to induce the formation of AgNPs. The characterization of as-synthesized AgNPs revealed that in a manner similar to other parts of plant exudates, the HRSF extract has better potential to facilitate the fabrication of nanoparticles in a time- and concentration-dependent manner. The kinetics of as-synthesized AgNPs was monitored using UV-Vis spectrophotometry. Next, we characterized the resultant AgNPs employing spectroscopic and other relevant techniques. The antibacterial and anti-biofilm potential of as-synthesized AgNPs were evaluated against a range of bacteria including caries causing *S. mutans*. Furthermore, we also assessed the anti-adherence potential of AgNPs against *S. mutans* adsorbed on orthodontic wires.

MATERIALS AND METHODS

All chemicals and reagents used in this study were of high purity (analytical grade) and procured from Sigma-Aldrich (St. Louis, MO, United States), unless mentioned otherwise. Silver nitrate (AgNO₃) was procured from Merck Research Laboratories Pvt.



Ltd. (India). Nickel–titanium (Ni-Ti) orthodontic wires were procured from Dr. Ziauddin Ahamd Dental College and Hospital, AMU, Aligarh, India. Luria Bertani (LB) broth, brain heart infusion (BHI), nutrient broth (NB), and agar powder were purchased from HiMedia (India). Fluorescein isothiocyanate (FITC) dye employed in fluorescence microscopy was purchased from Sigma-Aldrich (St. Louis, MO, United States). The bacterial strains were procured from ATCC, MTCC, and JNMCH, AMU, Aligarh. All the experiments were conducted with log-phase culture isolates.

Hibiscus rosa-sinensis Flower Extract Preparation

Fresh flowers of *Hibiscus rosa-sinensis* were collected from the Horticulture Nursery, AMU, Aligarh, India, and washed several times with deionized water. A known volume of distilled water (100 ml) was mixed with 10 g (wet weight) of thoroughly washed *HRS* flowers. The mixture was boiled till the original volume of aqueous suspension was reduced to 50 ml and filtered using Whatman No. 1 filter paper. The resulting *HRS* flower extract was used in the synthesis of as-fabricated AgNPs. Similarly, *HRS* buds and leaf extracts were prepared and employed in the fabrication of AgNPs.

Synthesis of AgNPs Using *HRS* Flower Extract

Increasing volumes (3–5 ml) of *HRSF* extract were added to 5 ml aqueous solution [10^{-3} M] of silver nitrate (AgNO_3). The final volume of each reaction mixture was made up to 10 ml by adding a sufficient amount of distilled water and was kept on a stirrer at 100 rpm overnight at room temperature (**Figure 1**). Synthesis of

AgNPs was also done by employing buds and leaf extracts of the *HRSF*. The as-synthesized AgNPs were characterized by various spectrophotometry-, transmission electron microscopy (TEM)-, and dynamic light scattering (DLS)-based analysis. The characterization and antibacterial activity data of buds and leaf extracts based on synthesized AgNPs are shown in the **Supplementary Table S1**.

Bacterial Strains

We used the following bacterial strains in the study:

Bacterial strains	Remarks
<i>Streptococcus mutans</i> [MTCC-497]	Gram-positive, resistant to ampicillin, azithromycin, ceftriaxone, and vancomycin
<i>Streptococcus mutans</i> [ATCC 700610/UA159]	Gram-positive, sensitive to erythromycin, rifampin (rifampicin) rifamycin, and streptomycin
<i>Streptococcus mutans</i> [Clinical isolate]	Gram-positive, NA
<i>Escherichia coli</i> [ATCC-25922]	Gram-negative, used as a control for antibiotic susceptibility assays
<i>Listeria monocytogenes</i> [ATCC 19115]	Gram-positive, quality control strain for Analytical Profile Index (API) products

Characterization of As-Synthesized AgNPs UV-Vis Spectroscopic Studies

A UV-Vis spectroscopic analysis of the as-synthesized AgNPs was performed to ascertain the biogenic reduction of precursor AgNO_3 . The double beam spectrophotometer (Jasco model V-750), operated at a resolution of 1 nm, was used to execute the analysis (Bhosale et al., 2014). The UV-Vis spectrum was recorded over the 200–800 nm range.

Determination of Particle Size by Dynamic Light Scattering

Dynamic light scattering (DLS) measurement was employed to determine the hydrodynamic size distribution of the particles. DLS measurements were analyzed by using Malvern Zetasizer Nano-ZS90 (ZEN3590, UK) to determine the average size and size dispersal of the as-synthesized AgNPs. The lyophilized powder was resuspended in PBS, and the solution obtained after passing through a 0.22- μm filter (Millipore) was subjected to various size determining measurements. The scattered light intensity was detected at 90° of the incident beam, and data analysis was performed in the default mode. The measured size was presented as the average value of 20 runs, with triplicate measurements within each run.

Transmission Electron Microscopy Measurement

The as-synthesized AgNPs were characterized by TEM. We also studied the effect of increasing volumes of the HRSF extract on the shape and size of the as-formed AgNPs with the help of the JEOL Transmission Electron Microscope at an accelerating voltage of 200 kV. A copper grid mesh, covered with the carbon-stabilized film, was employed to analyze the as-synthesized AgNPs. The uranyl acetate (2% w/v) solution was used for negative staining of the sample.

Zeta Potential Determination

For the determination of zeta potential of as-synthesized AgNPs, Malvern Zetasizer Nano-ZS90 (ZEN3590, UK) was used. Reconstitution of the samples was carried out in 5 mM phosphate buffer, pH 7.4, and the electrophoretic mobility was measured in the electrophoresis cell. The samples were run in triplicate to determine the zeta potential.

Fourier Transform Infrared Spectroscopy Measurement

FTIR spectra of as-synthesized AgNPs was analyzed on an FTIR spectrophotometer (PerkinElmer, UK) in the diffuse reflectance mode operating at a resolution of 4 cm^{-1} (Iravani et al., 2014). The spectra of AgNPs and HRSF extract were taken between 4,000 cm^{-1} and 400 cm^{-1} . As-synthesized AgNPs were co-prepared again along with KBr crystals as a beam splitter.

Anti-Bacterial Potential of As-Synthesized AgNPs as Revealed by the Zone of Inhibition Assay

The bactericidal activity of the as-synthesized AgNPs was assessed by employing the agar well diffusion method. Various bacterial strains such as *Listeria monocytogenes*, *Streptococcus mutans*, and *Escherichia coli* were used in the study. The bacterial strain *S. mutans* MTCC-497 (Institute of Microbial Technology, Chandigarh, India) was cultured in the brain heart infusion (BHI) broth (HiMedia Labs, Mumbai, India) at 37°C. We also used *S.*

mutans serotype c strain (ATCC 700610/UA159) to assess the antibacterial potential of as-synthesized AgNPs. Next, we determined the antibacterial potential of as-synthesized AgNPs against standard *E. coli* (ATCC-25922). The antibacterial potential of as-synthesized AgNPs was also established against *L. monocytogenes* ATCC 19115. The clinical isolate of *S. mutans*, used in the study, was a kind gift from Prof. Shahid of the Department of Microbiology, JNMC, AMU, Aligarh.

The nutrient broth was used for subculturing of the pure culture of *S. mutans*, *E. coli*, and *L. monocytogenes*. They were grown overnight to attain the colony-forming unit (CFU) count of $\sim 10^6$ units per ml. An aliquot of 100 μl , from overnight grown culture, was spread uniformly on nutrient agar plates by using a sterile plastic spreader.

The agar plates, inoculated with *S. mutans*, were cocultured with the AgNP-Ni-Ti orthodontic wire. The uncoated and plain AgNO₃-coated Ni-Ti orthodontic wires were used as the control. The plates were incubated at 37°C, and the zone of inhibition was observed after the stipulated time period of 24 h.

In the next set of experiments, the agar plates were first exposed with *E. coli* and *L. monocytogenes* followed by punching of the wells using a punching machine. Subsequently, an increasing amount of as-synthesized AgNPs (1 mg/ml stock solution) or standard antibiotic, vancomycin (control), was dispensed into various wells in a given agar plate. The plates were incubated at 37°C, and the zone of inhibition was determined by measuring the clear region around each well after the stipulated time period of 24 h.

Anti-Biofilm Potential of As-Synthesized AgNPs Employing XTT Assay

The anti-biofilm potential of as-synthesized AgNPs was established by employing the XTT assay, which is performed to analyze the presence of viable cells. The principle of the assay involves the cleavage of the tetrazolium salt XTT (2,3-bis(2-methoxy-4-nitro-5-sulfophenyl)-5-{phenylamino}carbonyl-2H-tetrazolium hydroxide) in the presence of an electron-coupling reagent, which ensues in the production of a soluble formazan salt. The XTT assay was performed following published protocols with minor changes as standardized in our lab. In brief, 100 μl of bacterial cell culture (1×10^8 cells/ml) was dispensed in each well of 96-well culture plates. The bacteria were allowed to form adherent mature biofilm in the presence of an increasing concentration of the as-synthesized AgNPs for 48 h. Just before the commencement of the assay, a solution of menadione (0.4 mM), which acts as an artificial electron transporter to reduce tetrazolium salt to formazan, was prepared and filtered.

The plate was incubated for the stipulated time period, followed by washing with PBS (200 μl). Next, the XTT reagent [2,3-bis(2-methoxy-4-nitro-5-sulfophenyl)-5-{phenylamino}carbonyl-2H-tetrazolium hydroxide (XTT) at a final concentration of 250 $\mu\text{g/ml}$] was dispensed to each test well of the plate followed by the addition of menadione solution (2 μl /well). The plate was further incubated for the next 4 h at 37°C in the dark. Next, the solution was transferred into a fresh plate to

assess the colorimetric change, and the absorbance was taken at 490 nm using an iMark microplate absorbance reader (BIORAD, United States). The XTT experiments were performed in triplicate to validate the data.

Effect of As-Synthesized AgNPs on the Adherence of *S. mutans* to Smooth Glass Surfaces in Presence of Sucrose

We studied the effect of as-synthesized AgNPs on the adherence of *S. mutans* on the smooth glass surface. We also assessed the effect of the presence of sucrose in the surrounding medium during AgNP-mediated inhibition of *S. mutans* adherence. The bacteria were cultured at 37°C for 24 h at an angle of 30° in a glass tube containing 10 ml of BHI with or without 5% (w/v) sucrose. The cultured tubes were also exposed to the sub-MIC concentrations of the AgNPs. The culture medium consisted of BHI (sucrose dependent) and without sucrose (sucrose independent). After stipulated incubation, the glass tubes were slightly rotated to decant the planktonic cells. Subsequently, the adhered cells were removed by adding 0.5 M of sodium hydroxide with stirring. The cells were thoroughly washed and suspended in saline. The adherence was determined spectrophotometrically at 600 nm. The percentage adherence was determined by using the following formula:

$$\text{percentage adherence} = (\text{O.D. of adhered cells} / \text{O.D. of total cells}) \times 100.$$

The effect of AgNPs on the cell surface hydrophobicity of *S. mutans* was determined by measuring its adhesion with hydrocarbon. The cells were grown in the BHI medium supplemented with 5% sucrose along with the increasing concentration of AgNPs. The cells were washed twice and suspended in sterile saline (0.85%) to adjust optical density (O.D.) at around 0.3 at 600 nm. A given volume of the cell suspension (3 ml) was mixed with 0.25 ml toluene. The tubes were stirred for 2 min and allowed to equilibrate at room temperature for 10 min. The cell suspension was kept aside to allow phase separation. We next determined the O.D. of the aqueous phase spectrophotometrically at 600 nm.

Hydrophobicity Index of As-Synthesized AgNP-Treated Bacterial Biofilm

Overnight cultured bacterial cells (treated and control) were suspended in 1 ml LB medium to obtain optical density (at a wavelength of 600 nm) at around 1.0 ± 0.01 . Furthermore, toluene (1 ml) was added to the suspension (both treated and control) and vortexed. The test tubes were incubated for 30 min to let the biphasic solution settle. Next, the optical density of the aqueous phase was measured, and the hydrophobicity index was calculated by using the following equation:

$$HI\% = [(A_i - A_f) / A_i] \times 100,$$

where A_i and A_f denote the initial and final optical densities of the aqueous phase. The adherence of the bacterial cells to the

organic solvent was evaluated to ascertain the hydrophobicity (Farkas et al., 2015).

Anti-Adherence Properties of As-Synthesized AgNPs

Sterilized Ni-Ti orthodontic wires were placed into three separate Eppendorf tubes containing fresh sterilized nutrient broth. Next, one of the two sets of orthodontic wires was co-incubated with as-synthesized AgNPs (50 µg/ml) and the other with aqueous AgNO₃ solution (50 µg/ml). The wire, incubated in media only, served as the control. The standardized suspension (1×10^8 cells/ml) of *S. mutans* was added to each Eppendorf tube (harboring orthodontic wire) and was incubated for 24 h at 37°C. Once the incubation period was over, wires were taken out and placed into fresh Eppendorf tubes containing PBS and subjected to sonication to remove adhered bacteria from wires. A known volume (100 µl) of the resultant bacterial suspension (diluted 100 times), collected post sonication, was spread on NB agar plates and incubated for 24 h at 37°C, and CFU/ml was calculated for each group.

Anti-Biofilm Activity as Revealed by Fluorescence Microscopy

S. mutans was cultured in the NB medium at 37°C overnight. An aliquot of log-phase bacterial culture (having 10^6 CFU/ml) was suspended in broth (500 µl) and dispensed on the sterile coverslip placed in wells of a multi-well polystyrene plate. The setup was left for 24 h at 37°C for the growth of biofilm. Mature biofilm was washed and incubated with AgNPs (50 µg/ml) suspension and AgNO₃ solution (50 µg/ml) for the duration of 3 h. An untreated mature biofilm was considered as a control. Coverslips were then fixed in 4% paraformaldehyde (PFA) followed by washing, and cells were then stained with the fluorescein isothiocyanate (FITC) dye. Stained coverslips were then washed with sterile PBS, and the anti-biofilm activity was observed under the Zeiss Axiocam Imager MRM M2 fluorescence microscope. Both the treated and control samples were observed under a fluorescence microscope (×40 magnification).

Quantification of Extracellular Glucan in Cultures With Sucrose

The phenol/H₂SO₄ method (Decker et al., 2011) was used to quantify the glucan in the cultured sample. *S. mutans* was incubated in media containing 1% sucrose both in the absence and presence of as-synthesized AgNPs for 20 h, after which the bacteria were recovered. Extracellular water-soluble glucan was isolated by employing ethanol precipitation of the supernatants from the recovered bacterial cultures. The remaining cell pellet was resuspended in 1 M NaOH and centrifuged to remove bacterial cells. Water-insoluble glucan was recovered by ethanol precipitation of the supernatant.

Assessment of Topographical Changes in Orthodontic Wires

Ni-Ti orthodontic wires were incubated with as-synthesized AgNPs (50 µg/ml) and aqueous AgNO₃ (50 µg/ml) for 24 h with mild and continuous shaking for homogenous adherence. Topographical changes on coated Ni-Ti orthodontic wires as compared to uncoated one (control) were assessed by scanning electron microscopy (JSM67500F, a JEOL model, Japan).

Cytotoxicity Assays

To facilitate the future plausible biomedical application, we assessed the cytotoxicity of the as-synthesized AgNPs against erythrocytes (RBCs) and PBMCs. It was done by performing an *in vitro* hemolysis assay of RBCs and killing of PBMCs employing the MTT assay as described later.

Hemolysis Assay

In brief, fresh blood was drawn from a healthy individual and mixed with an anticoagulant solution (EDTA) before being centrifuged at 8,000 rpm for 10 min at 4°C. The buffy coat formed after centrifugation was discarded, and the erythrocyte was collected and washed with a diluted isotonic buffer (20 mM PBS) to prepare 50% hematocrit. The degree of hemolysis was determined by incubating RBC suspensions with various concentrations of AgNPs for 1 h at 37°C. All samples from the incubated solutions were centrifuged at 10,000 rpm for 10 min, the resulting supernatant was collected and the absorbance was recorded at 576 nm for released hemoglobin by UV-VIS spectroscopy. The percentage of hemolysis was determined by the following equation:

$$\% \text{Hemolysis} = \left[\frac{\text{Abs}_T - \text{Abs}_C}{\text{Abs}_{(100\%)} - \text{Abs}_C} \right] \times 100.$$

In the discussed equation, Abs_T represents the absorbance of the supernatant from samples incubated with AgNPs, and Abs_C is the absorbance of the supernatant from control (PBS). Abs_(100%) represents the absorbance in the presence of 1% Triton X-100 as a positive control.

MTT Assay

The MTT assay was performed for assessing cell viability. MTT (Thiazolyl Blue Tetrazolium Bromide), is a yellow dye that is converted into formazan, by the activity of the mitochondrial dehydrogenase. In brief, peripheral blood mononuclear cells (PBMCs) were isolated following the standard protocol as standardized in our lab. Next, we dispensed 10⁴ cells per well in 96-well plates and incubated in the complete medium overnight. The next morning, the medium was aspirated and cells were incubated with varying concentrations of AgNPs at 37°C for 24 h followed by further 4-h incubation with the MTT dye (5 mg/ml in PBS). The reaction mixture was aspirated and the resulting formazan crystals were dissolved by adding 200 µl of DMSO. After 10 min, absorbance was read at 570 nm using an iMark microplate absorbance reader (BIORAD, United States). Untreated sets served as controls which were performed simultaneously under identical conditions. The MTT experiments were performed in triplicate to validate the data.

Finally, OD values of culture were converted into percentage viability by using the following formula:

$$\text{cell viability} (\%) = \left[\frac{\text{OD}_{\text{sample}}}{\text{OD}_{\text{Control}}} \right] \times 100.$$

Statistical Analysis

Data were analyzed by one-way and two-way ANOVA to assess the differences among groups. Statistical calculations were performed with the help of GraphPad Prism version 8.0. Significance was indicated as *** for $p < 0.001$; ** for $p < 0.01$, and * for $p < 0.05$.

RESULTS

Hibiscus Flower Extract Mediated Synthesis of Silver Nanoparticles

The potential of *HRSF* extract to synthesize nanoparticles was established by evaluating its ability to convert silver salt to as-synthesized silver nanoparticles. The aqueous silver ions were exposed to the *HRSF* extract. The color of the reaction mixture changed from light pinkish-red to dark brown (**Supplementary Figure S1**). The color transformation corresponds to the characteristic surface plasmon resonance (SPR) effect of different size silver nanoparticles. The SPR analysis establishes *HRSF*-mediated synthesis of AgNPs.

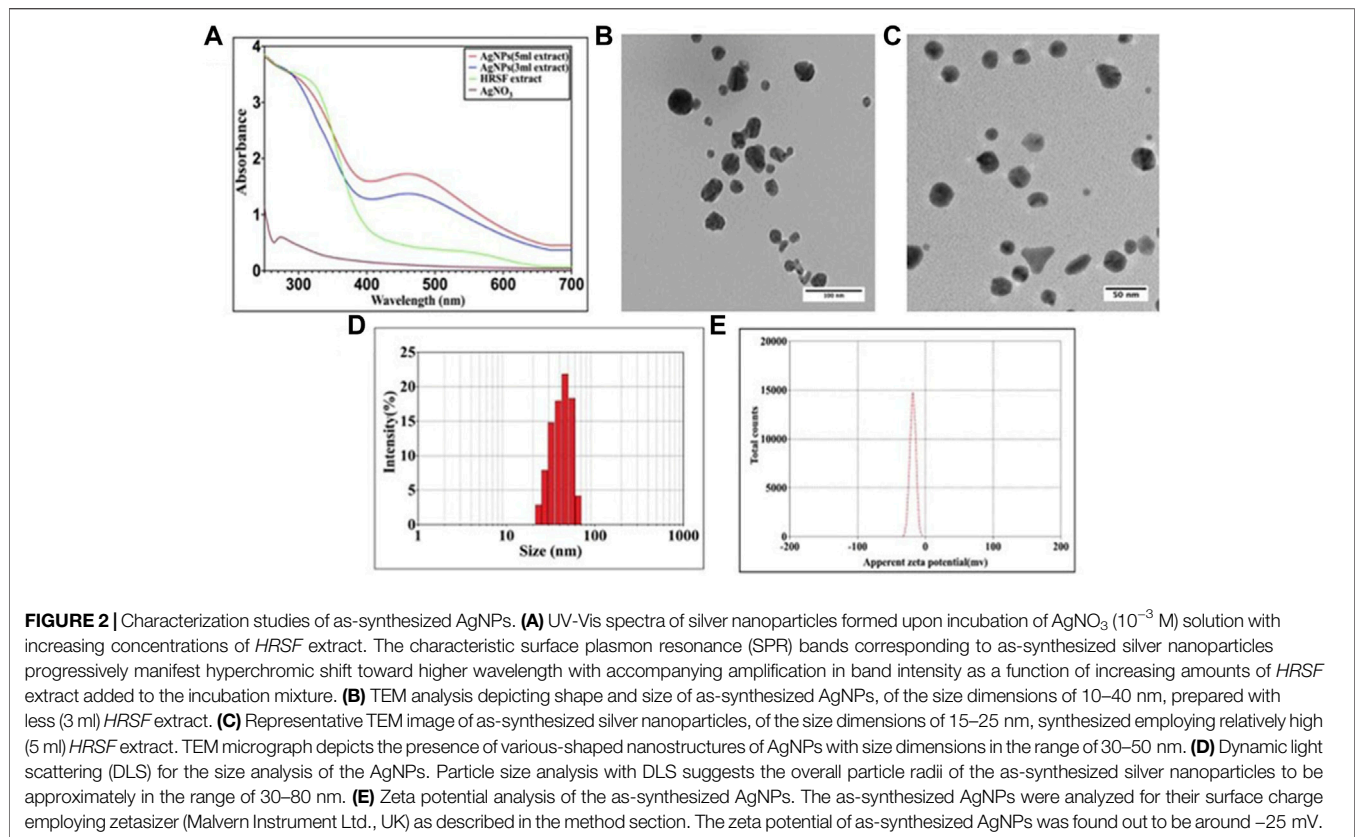
UV-Vis Spectroscopic Analysis of Silver Nanoparticles

The optical properties of the as-synthesized AgNPs were determined by employing surface plasmon absorption spectroscopy. The SPR properties usually depend on the shape of the NPs population. At the outset, a UV-Vis absorption spectroscopic technique was used to analyze the synthesis of the nanoparticles. **Figure 2A** shows the UV-Vis absorption spectra recorded for as-synthesized silver nanoparticles harvested after 24 h of the reaction (upon treatment with 3 ml of *HRSF* extract). The results indicate that the reaction solution displayed an absorption maximum at about 460 nm that can be attributed to the SPR of the as-synthesized silver nanoparticles (Lim, 2014). It was observed that with the increase in time, the silver nanoparticle synthesis rate also increased (**Supplementary Figure S2**). Although the wavelength maximum was stably positioned at 460 nm, the intensity steadily increased with time and eventually got saturated after 24 h.

We also studied the kinetics of silver nanoparticle synthesis upon incubation of AgNO₃ with increasing content of *HRSF* extract. The synthesis of AgNPs augmented upon increasing the concentration of plant extract in the reaction medium. The increase in *HRSF* content (3 vs. 5 ml *HRSF* extract) resulted in an upsurge in absorbance at 460 nm (**Figure 2A**).

TEM and DLS Analysis

The green synthesis of silver nanoparticles was further confirmed by representative TEM images of silver nanoparticles generated



employing increasing amounts of flower extract for their synthesis. The shape of the particles was found to be dependent on the concentration of flower extract. Higher abundance of *HRSF* extract favored the occurrence of a largely homogenous population of small-sized nanoparticles. At lower concentrations of flower extract various triangular, hexagonal, and ovoid shaped particles in the size range 10–40 nm (Figure 2B) were seen coexisting. However, as the concentration of *HRSF* extract was increased, the average diameter of the silver nanoparticles was found to decrease as evidenced by the occurrence of spherical particles (15–25 nm) at higher concentrations of *HRSF* extract (Figure 2C). Also, as the flower extract concentration increased, the total number of particles in a given volume increased simultaneously as seen in the TEM micrograph (Figure 2C). Initially, the increase in the *HRSF* extract causes the nanoparticles to be formed in the range of 30–50 nm. This is more evident from the fact that a higher concentration of flower extract led to the synthesis of the large number of isomorphous spherical nanoparticles of small dimensions (20–30 nm), which is accompanied by a decrease in the number of large-sized compounds with the size range of 30–50 nm.

For the determination of the particle size of as-synthesized AgNPs in an aqueous buffer, the dynamic light scattering (DLS) analysis was carried out. To have better information pertaining to the size distribution of as-synthesized AgNPs, DLS is performed in conjunction with the TEM analysis. Analysis of the *HRSF* extract-mediated synthesized AgNPs' dynamic light scattering

(DLS) pattern showed the average size of as-synthesized AgNPs to be around 30–80 nm with a polydispersity index (PDI) of 0.28 (Figure 2D). The TEM analysis revealed the morphology of the as-synthesized AgNPs to be spherical/ovoid and having a size range of around 30–50 nm. The discrepancy in the size as determined by DLS versus TEM analyses is usually explained on the basis of the hydrodynamic diameter of AgNPs, which correspond to the size of the particles suspended in the liquid medium (Figure 2 B&C).

Surface Charge of AgNPs as Measured by Zeta Potential

Zeta potential is a physical property which relates to the net surface charge of the nanoparticles. Depending upon the magnitude and nature of the charge, the particles may repel each other (because of the Coulomb explosion force) eventually preventing agglomeration of the as-synthesized nanoparticles. The stability of NPs has been correlated well with the zeta potential ranging from +30 mV to -30 mV. The as-synthesized AgNPs were found to have zeta potential of around -25 mV [Figure 2E].

FTIR Analysis

FTIR spectroscopy was performed to characterize the putative biomolecules (organic and inorganic functional groups) responsible for the reduction of Ag^+ ions and the stabilization of reduced silver nanoparticles to prevent agglomeration and

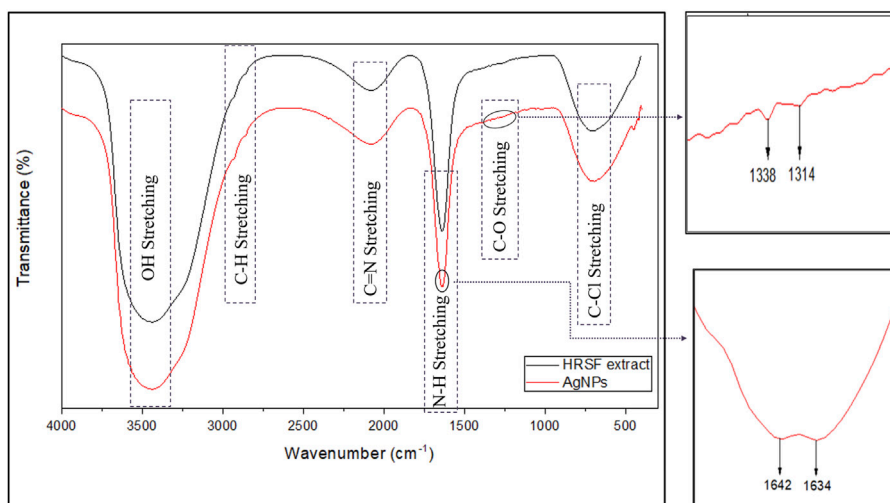


FIGURE 3 | FTIR spectrum of as-synthesized AgNPs. FTIR spectroscopy was used for the characterization of functional organic and inorganic groups sourced from *HRSF* extract responsible for the formation and stabilization of AgNPs.

their capping in the aqueous medium. The FTIR spectra of *HRSF* extract and the as-synthesized AgNPs are shown in **Figure 3**. Both the spectra showed bands at 3,446, 2,927, 2,856, 2,074, 1,638, and 708, cm^{-1} . The strong peak at 3,446 cm^{-1} corresponds to the O–H stretching of alcoholic and phenolic groups. The absorption bands in the region of 3,000–2,700 cm^{-1} are characteristic of the C–H group in alkanes. So, the peaks at 2,927 and 2,856 cm^{-1} with medium to weak intensity suggest aliphatic and aromatic C–H stretching. The peak at 2,074 cm^{-1} accounts for C=N stretching of R–N=C=S. The sharp band at 1,638 cm^{-1} can be assigned to the amide I bond of proteins in *HRSF* extract as the band in the region of 1,680–1,500 cm^{-1} has been shared between the amide bond of protein (sourced from flower extract) and also due to stretching vibrations in the secondary structure of protein resulting in the formation of two new peaks at 1,642 and 1,634 cm^{-1} (as clearly revealed in the zoomed-in image) in silver nanoparticles. The lower frequency bands at 708 cm^{-1} can be assigned to C–Cl stretching with C–H bending vibrations out-of-plane. In the IR spectrum of the AgNPs, new bands are observed at 1,338 and 1,314 cm^{-1} (shown as the zoomed-in image), corresponding to the C–O stretching.

Antibacterial Potential of AgNPs as Assessed by Agar Well Diffusion Method

The antimicrobial activity of AgNPs was assessed against all three strains of *S. mutans* (MTCC-497, ATCC-700610, and the clinical isolate) using the agar well diffusion assay (data pertaining ATCC-700610 and clinical isolate is presented as **Supplementary Figure S3** in the supplementary section). The as-synthesized AgNPs were found to be effective against all the strains under study, but the data shown in the whole study corresponds to a resistant strain of *S. mutans*, MTCC-497. The zone of inhibition (in mm) around each well containing AgNPs was assessed (**Figure 4**). We also determined the

antibacterial activity of the as-synthesized AgNPs against *E. coli* and *L. monocytogenes*. The AgNPs exhibited significant antibacterial activity against all the tested organisms. Ni-Ti orthodontic wires were coated with as-synthesized AgNPs or AgNO_3 solution. The impregnated wires were placed on the agar plate that was previously inoculated with resistant isolates of *S. mutans*. The wire impregnated with AgNPs (50 $\mu\text{g}/\text{ml}$) showed significant *S. mutans* inhibition (clear zone of inhibition) as compared to AgNO_3 (50 $\mu\text{g}/\text{ml}$) solution-coated wire (**Figure 5**).

Anti-Adherence Potential of As-Synthesized AgNPs

The anti-adherence potential of as-synthesized AgNPs was deduced by incubating Ni-Ti orthodontic wires with AgNPs and their further incubation with *S. mutans*. It was found that there was maximum bacterial load in terms of (CFU/ml), as shown in the case of uncoated wires (control), while wires coated with aqueous AgNO_3 solution and as-synthesized AgNPs shown less bacterial load than the control. The least bacterial load was found in the case of wires impregnated with AgNPs as compared to both uncoated and AgNO_3 coated wires (**Figures 6A,B**).

Anti-Biofilm Potential of As-Synthesized AgNPs Employing XTT Assay

The as-synthesized AgNPs inhibited adherence of *S. mutans* to the surface of glass tubes. The as-synthesized AgNPs inhibited both sucrose-independent and sucrose-dependent adherence of the treated *S. mutans* bacteria. The inhibition was more pronounced in sucrose-dependent adherence as compared to the sucrose-free medium. The as-synthesized AgNPs inhibited the *S. mutans* biofilm formation in a dose-dependent manner

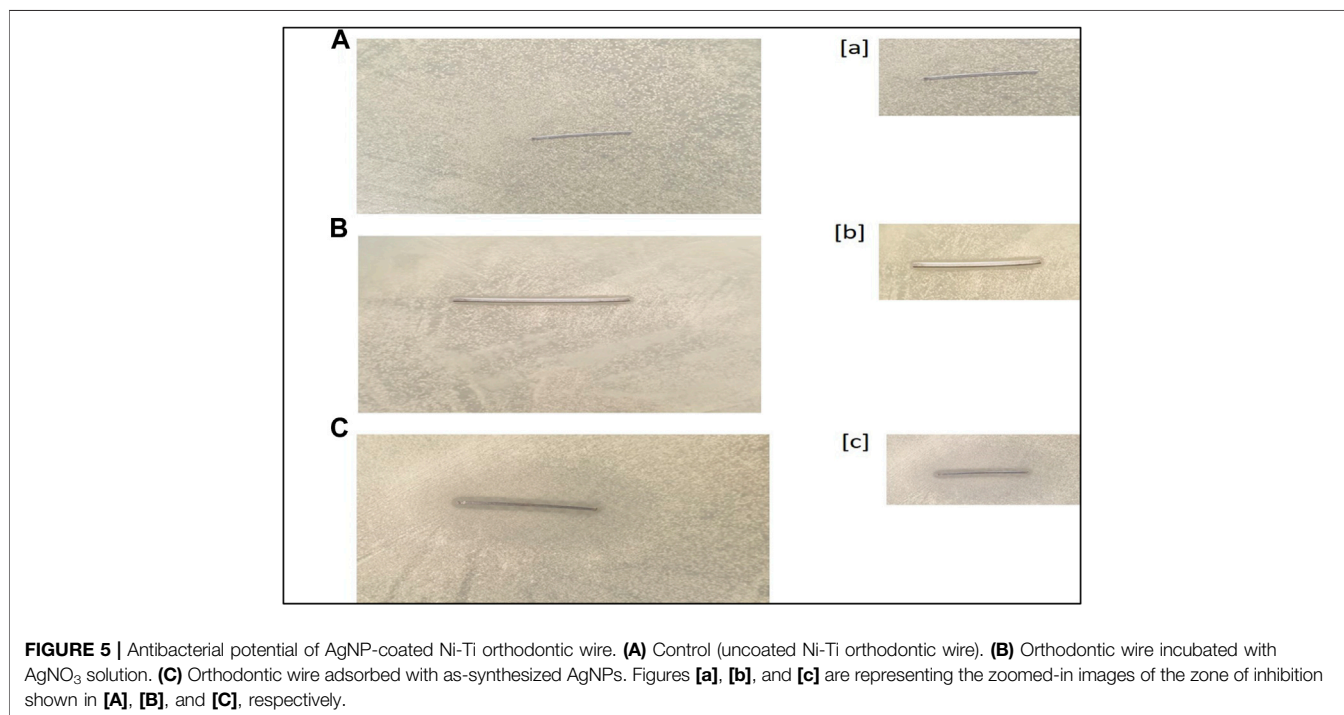
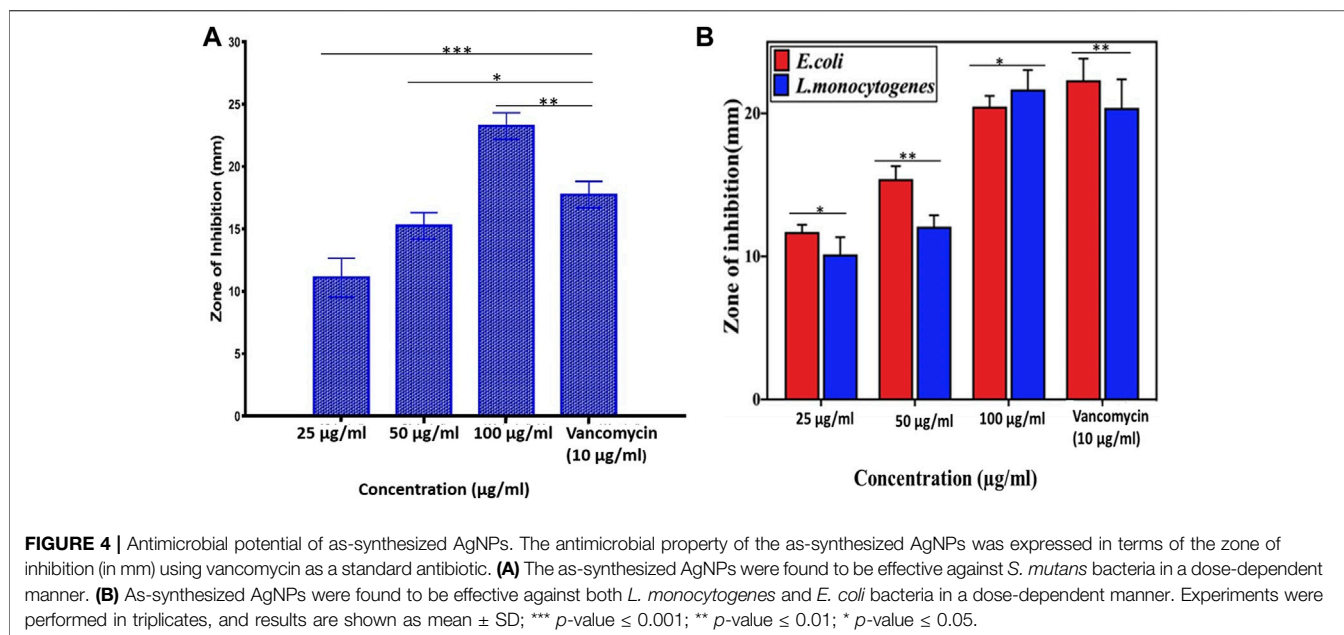


(Figure 7A). The AgNPs at a concentration of around 25 $\mu\text{g/ml}$ inhibited around 50% of the formed biofilm.

AgNPs Mediated Inhibition of *Streptococcus mutans* Hydrophobicity

The as-synthesized AgNPs were found to inhibit cell surface hydrophobicity of *S. mutans* in a concentration-dependent manner, as shown in Figure 7B. The as-synthesized AgNPs

reduced the hydrophobicity to more than 50% at a concentration of $\sim 100 \mu\text{g/ml}$. On the other hand, the precursor AgNO_3 solution failed to reduce the hydrophobicity.

We also determined the anti-biofilm potential of as-synthesized AgNPs against less susceptible isolates of *L. monocytogenes* and *E. coli*. The increasing amount of AgNPs (ranging from 1.56 to 200 $\mu\text{g/ml}$) was dispensed in each well of the microtiter plate. Subsequently, the plate was inoculated with a bacterial strain (for 24 h) specified in the Method section. It can

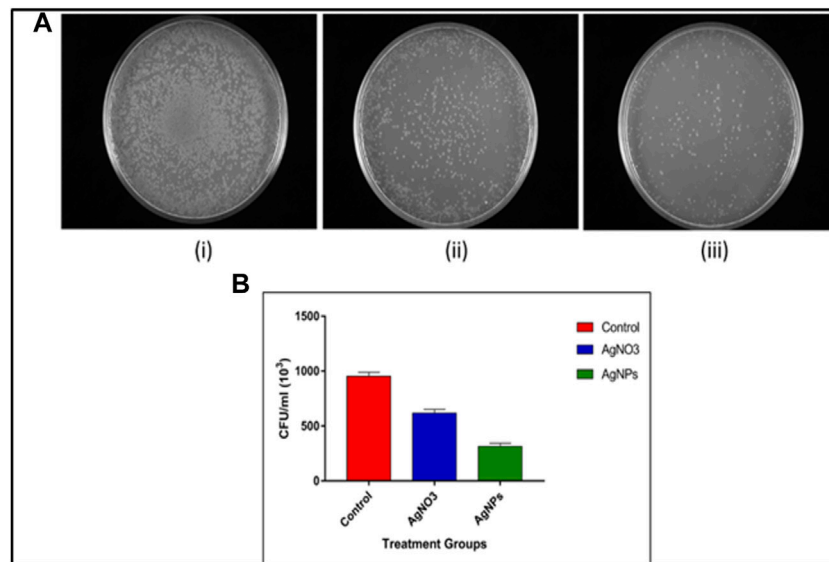


FIGURE 6 | Anti-adherence properties of AgNP-coated Ni-Ti orthodontic wires. **(A)** Adhered *S. mutans* bacterial population collected from **(i)** uncoated orthodontic wire, **(ii)** wire incubated with aqueous AgNO₃ solution (50 µg/ml), and **(iii)** wire adsorbed with as-synthesized AgNPs (50 µg/ml). **(B)** Representative bar graphs corresponding anti-adherence property of AgNP-impregnated Ni-Ti orthodontic wires. The bacterial burden in terms of CFU/ml corresponding adhered bacterial population present on the surface of Ni-Ti orthodontic wires. Control-uncoated Ni-Ti orthodontic wire, AgNO₃ (aqueous solution)-coated Ni-Ti orthodontic wire, and as-synthesized **AgNP**-coated Ni-Ti orthodontic wire.

be inferred from the results that the biologically synthesized AgNP-based formulation was successful in inhibiting the drug-resistant bacterial biofilm (less susceptible against gentamicin), as compared to the negative control (Figure 7E). The adherence potential of bacterial cells can be attributed to the high hydrophobicity associated with the bacterial cell surface (Hu et al., 2019). The percentage of hydrophobicity index for *E. coli* (less susceptible isolate) decreased from ~58% to ~34% on treatment with as-synthesized AgNPs. Similarly, the hydrophobicity index for less susceptible *L. monocytogenes* isolate decreased from ~64% to ~43% (Figure 7F).

As-Synthesized AgNPs Inhibited Glucan Synthesis in the Treated *S. mutans* Cells

We determined the potential of the as-synthesized AgNPs to inhibit glucan synthesis in the treated *S. mutans*. The AgNPs efficiently inhibited glucan synthesis in a concentration-dependent manner. The AgNPs inhibited around 50% glucan synthesis at around 100 µg/ml concentration (Figure 7C).

Anti-Biofilm Activity as Revealed by Fluorescence Microscopy

To ascertain the anti-biofilm potential of the as-synthesized AgNPs, we assessed *S. mutans* (drug-resistant MTCC-497)-mediated synthesis of biofilm on the glass surface in the presence of AgNO₃ solution or AgNPs. The fluorescence microscopy revealed the formation of mature biofilm when *S. mutans* was cultured in absence of AgNPs. The synthesis of profuse biofilm could be attributed to the unhindered

proliferation of untreated cells. On the other hand, the treatment with AgNPs resulted in the inhibition of biofilm formation on the glass surface (Figure 8).

Assessment of Topographical Changes in Orthodontic Wires

Surface morphology or the topographic conditions of Ni-Ti orthodontic wires was studied by the SEM analysis (Figure 9). As revealed by SEM micrographs, the surface of AgNP-coated Ni-Ti orthodontic wires showed less irregular topography in comparison to both aqueous AgNO₃ solution coated and uncoated wires. The uncoated Ni-Ti orthodontic wires were found to possess a significant number of well-distributed irregular cavities and a large number of pores on their surface. On the other hand, fewer topographic irregularities were observed on Ni-Ti wires that were coated with AgNO₃ solution.

Cytotoxicity Assays

In order to investigate biocompatibility, we carried out toxicity assays on RBCs (hemolytic assay) and PBMCs (MTT assay). The obtained results revealed that even at a very high dose (256 µg/ml) of AgNP exposure, only around 30% of RBCs were hemolyzed, as shown in Figure 10A; similarly, for PBMCs, it showed around 77% cell viability after exposure to 128 µg/ml (Figure 10B). However, exposure of cells to increasing doses of AgNPs resulted in decreased cell viability. The findings indicate that AgNPs are a stable and non-toxic entity with significant antibacterial action that does not cause toxicity in the host cells.

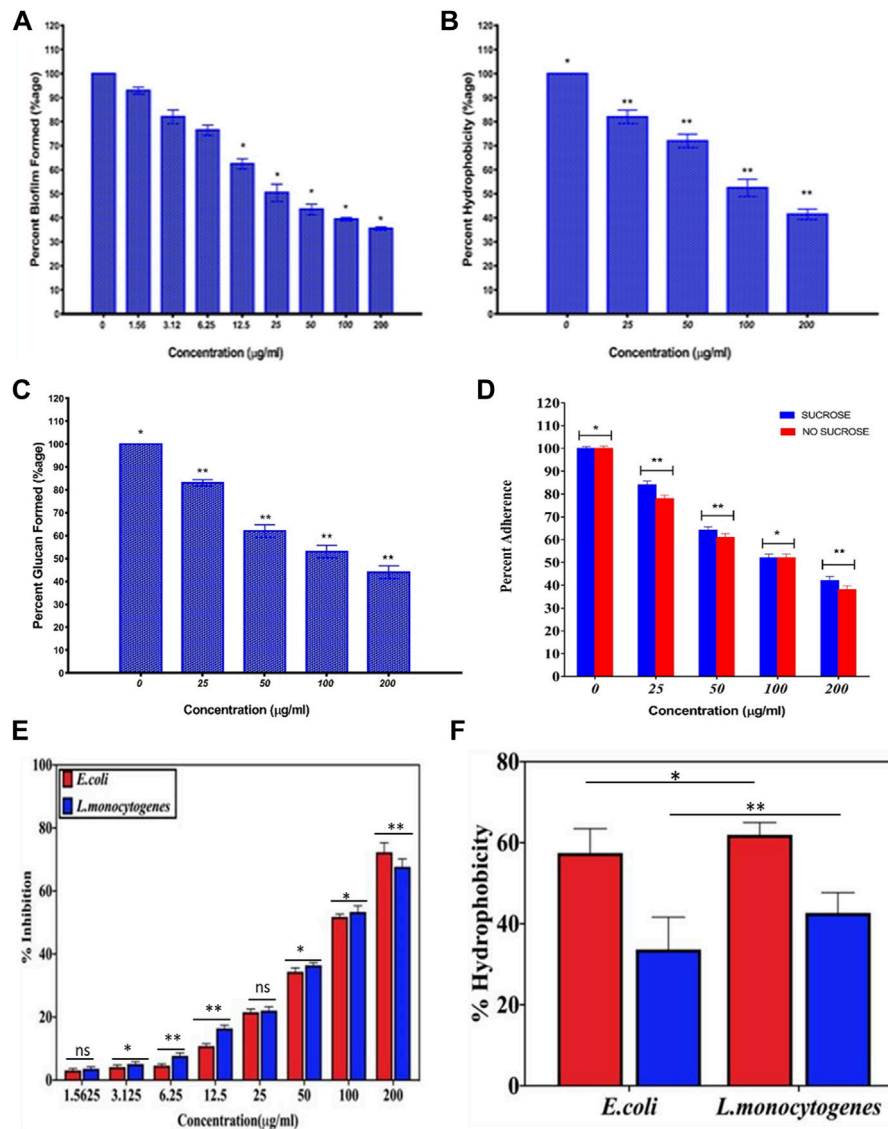


FIGURE 7 | Anti-biofilm potential of as-synthesized AgNPs. The anti-biofilm property of as-synthesized AgNPs against *S. mutans* was revealed by employing (A) XTT assay and (B) Hydrophobicity assay. (C) As-synthesized AgNPs were able to inhibit glucan synthesis by *S. mutans*, and it also resulted in its (D) decreased adherence potential on the glass surface. The anti-biofilm property of as-synthesized AgNPs against sensitive and resistant isolates of both *Listeria monocytogenes* and *Escherichia coli* bacteria as revealed by employing (E) XTT assay and (F) hydrophobicity assay. The hydrophobicity assay was performed against sensitive (blue) and resistant isolates of the two bacteria. Experiments were performed in triplicates, and results are shown mean \pm SD; ** p -value \leq 0.01; * p -value \leq 0.05; ns = non-significant.

DISCUSSION

The recent upsurge in the emergence of microbial isolates, which have the potential to withstand the antibiotic onslaught, has inflicted a serious impact on the strategies employed in the treatment of various infectious diseases. The failure of antibiotics in killing disease-causing microbes calls for the development of alternate modes of therapy. In general, the survival of the pathogenic microbes in the oral cavity depends on their successful adhesion and ability to develop into biofilms on dental surfaces. The as-synthesized biofilm protects microbes

from environmental challenges and helps in their growth and propagation. The microbial biofilm can develop on dental implants leading to peri-implantitis which is considered to be the main reason for implant failure.

Interestingly, metal-based nanoparticles offer a salvage strategy to treat the oral infection. In this regard, silver-based nanoparticles (AgNPs) can successfully control infection (Dutta et al., 2016). In the present study, we have synthesized AgNPs using an eco-friendly green synthesis method. The reduction of Ag^+ (metal salt) into Ag^0 (metallic nanoparticle) and its subsequent capping (to prevent aggregation) was executed

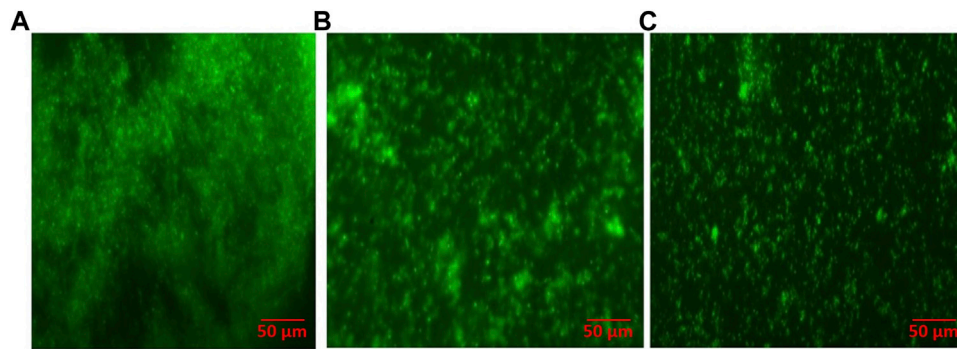


FIGURE 8 | As-synthesized AgNPs inhibit *S. mutans* biofilm as revealed by fluorescence microscopy (40×). **(A)** Mature, untreated biofilm of *S. mutans*; **(B)** biofilm inhibition upon treatment with aqueous AgNO_3 solution; and **(C)** biofilm inhibition upon treatment with as-synthesized AgNPs.

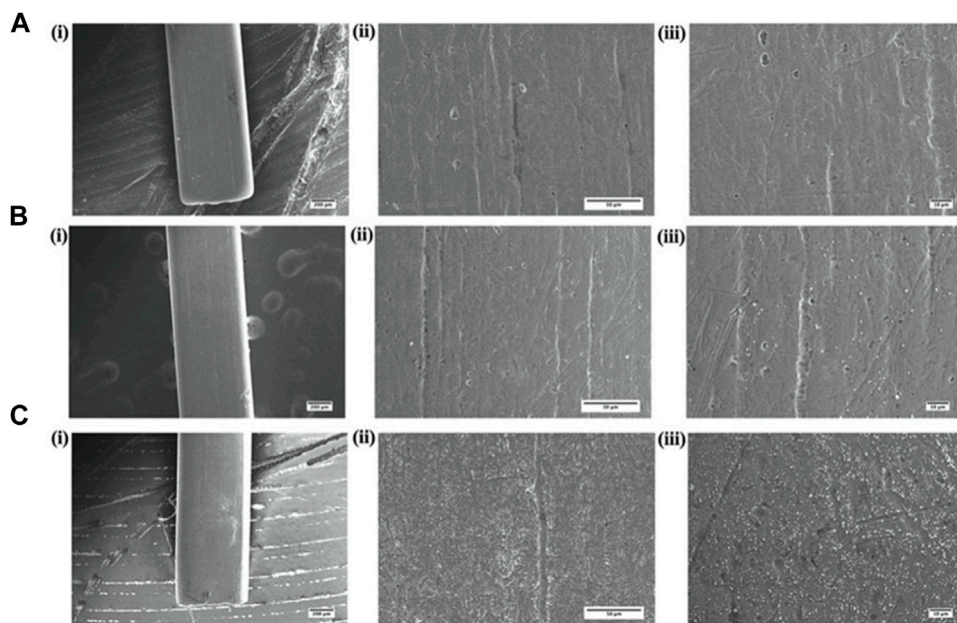


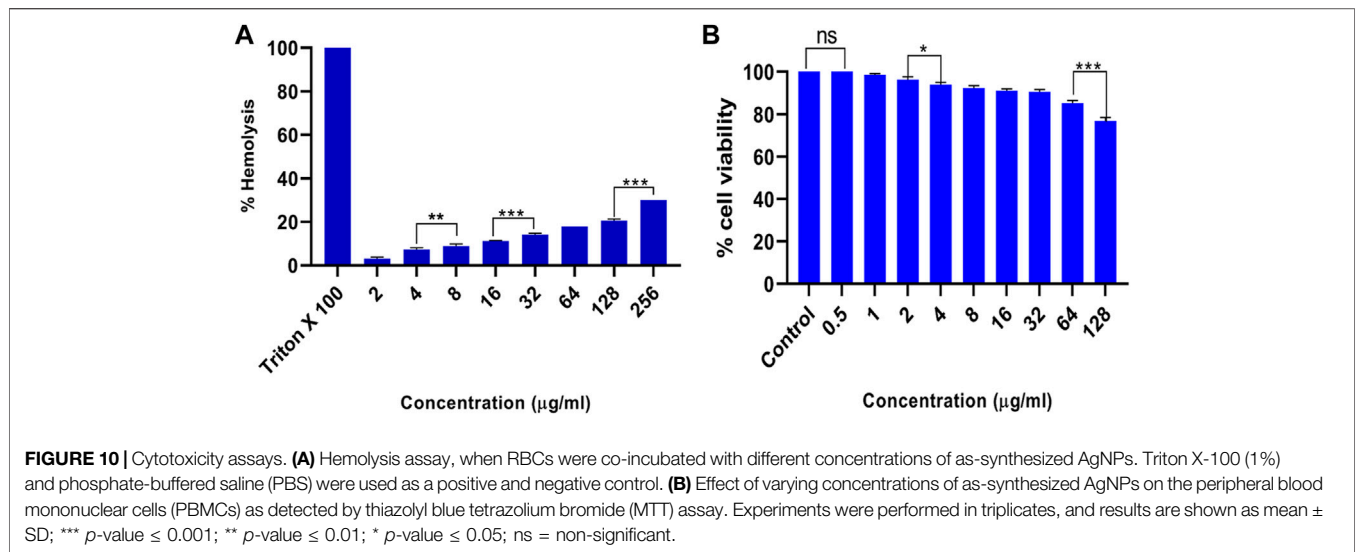
FIGURE 9 | Surface characterization of AgNP-coated Ni-Ti orthodontic wire. Scanning electron micrographs showing graded magnifications of **(A)** uncoated wire, **(B)** wire coated with aqueous AgNO_3 solution, and **(C)** wire coated with as-synthesized AgNPs, while **(i)**, **(ii)**, and **(iii)** represent 55×, ×500, and ×1000 magnifications, respectively.

employing *HRSF* extract (**Figure 1**). AgNPs were also synthesized by employing other parts of the *HRSF* such as bud and leaf extracts, characterized and evaluated for their potent antibacterial activity. However, in the present study, we have focused mainly on *HRSF* extract-based synthesized AgNPs as it was found more effective for the plausible antibacterial activity and anti-adherence activity on the surface of Ni-Ti orthodontic wires against *S. mutans*.

To begin with, first, we characterized the as-synthesized AgNPs for their physicochemical attributes. To track the progress of the fabrication of biogenic nanoparticles, TEM and UV spectrophotometric studies were carried out. The *HRSF*-mediated biological synthesis led to the formation of spherical

AgNPs, with size distribution in the range of 15–40 nm. The DLS analysis suggested the size dimension of as-synthesized AgNPs in the range of 30–80 nm. The discrepancy in the observed average size of the as-synthesized particles determined by the above specified two different methods can be attributed to the technique used in size determination (Wang L et al., 2017).

The as-synthesized AgNPs were found to exhibit characteristic SPR showing absorption peak at 460 nm. In accordance with the Mie theory, a single SPR band is obtained in the case of spherical nanoparticles. The FTIR spectroscopy also suggested the formation of a new micro-ambiance corresponding to functional groups of the parent compounds present in *HRS* flower extract.



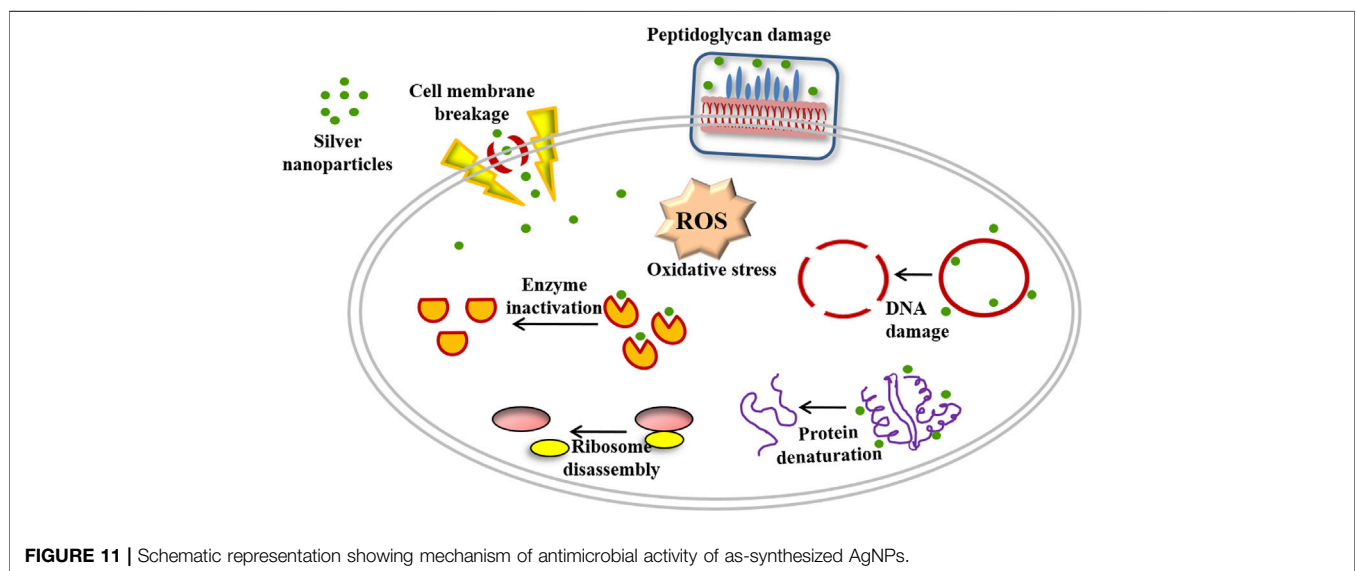
The zeta potential values ranging from +30 to -30 mV are supposed to help in maintaining the stability of the related nanoparticles (Mourdikoudis et al., 2018). Incidentally, the as-synthesized AgNPs were found to have zeta potential around -25 mV. This suggests that HRSF extract mediated the synthesis of stable AgNPs.

The characterization (UV-Vis spectrum, DLS, and zeta potential) and antibacterial data [MIC value and ZOI study against *S. mutans* (MTCC-497)] for the AgNPs synthesis employing HRS bud and leaf extracts are shown in the supplementary section (Supplementary Table S1).

Keeping into consideration the usefulness of silver nanoparticles in the treatment of a range of microbial infections, we tested their anti-biofilm potential against various other classes of bacteria in addition to *S. mutans*. Fabrication of nanoparticles employing biological methods, that is, green

synthesis, offers additional benefits in terms of biocompatibility and bioavailability. We made an elaborated effort to ascertain the effect of as-synthesized AgNPs against both resistant and sensitive bacterial isolates. The anti-biofilm activity, as revealed by the XTT assay, suggests that as-synthesized AgNPs can significantly inhibit less susceptible isolates of *S. mutans*, *E. coli*, and *L. monocytogenes*. The observed effectiveness of as-synthesized AgNPs to kill both sensitive and less susceptible isolates of bacteria has great relevance in the present scenario where drug resistance crisis by microbes is posing a great health concern. Moreover, as-synthesized AgNPs were also shown to inhibit glucan synthesis by *S. mutans*.

We established the potential of as-synthesized AgNPs to inhibit bacterial growth on orthodontic appliances. The AgNPs deposited on the surface of experimental dental appliances



including Ni-Ti orthodontic wires showed strong antimicrobial properties. In general, orthodontic appliances serve as a favorable site for *S. mutans* to adhere by forming a bacterial biofilm on their surface. However, if coated with AgNPs, they showed significant anti-adherence properties as well. The electron microscopic studies further established the anti-adherence activity of the AgNPs on orthodontic wires (**Figure 9**).

While the practice of establishing antimicrobial activity of AgNPs against various pathogens is a common feature, the studies pertaining to the anti-adherence potential of AgNPs in the context of orthodontic wires are limited (Sun et al., 2014). This makes the present approach more relevant as we have demonstrated that coating of AgNPs onto the surface of orthodontic wire imparts anti-adherence properties to the later. This observation is very interesting and has great relevance as orthodontic wires and other related dental appliances are very prone to be contaminated by various oral bacteria including *S. mutans*.

Earlier studies have suggested that AgNPs have the ability to release silver ions that have the potential to kill target bacterial cells (Francolini et al., 2017). The observed anti-adherence property of the AgNPs may be attributed to the fact that they can penetrate the cell wall of associated bacteria and also prevent the production of extracellular polysaccharides (**Figure 11**) to check bacterial adhesion on orthodontic wires.

The immersion of orthodontic wire in AgNP suspension, followed by their interaction with *S. mutans* on the agar plate ensued in killing (clear zone of inhibition) of bacteria present in the surrounding ambiance. There is a possibility that AgNPs may interact with thiol or amino acid residues of various crucial enzymes and eventually lead to inhibition of the bacterial cells (Mohanty et al., 2012). The large surface area of as-synthesized AgNPs is likely to facilitate the inhibition of various metabolically active enzymes (**Figure 11**). Moreover, AgNPs have also been reported to facilitate the generation of reactive oxygen species under the oxygen atmosphere (Rizzello and Pompa, 2014). The potential of as-generated ROS to act on proteins and DNA-based macromolecules has been considered detrimental to the live bacterial cells (**Figure 11**) (Li et al., 2013). The higher adhesion of *S. mutans* can be attributed to the surface morphology of the uncoated (bare) orthodontic wires

(**Figure 5**). The rougher surfaces are known to encourage biofilm formation and support greater adherence (Ramamany and Lee, 2016; Wang Y et al., 2017). In contrast, the treatment with AgNPs minimizes irregular cavities and the undulating surface of orthodontic wires, thereby minimizing adherence of *S. mutans* (**Figure 5** and **Figure 9**).

Finally, we can conclude that as-synthesized AgNPs showed remarkable antibacterial potential against both resistant and sensitive isolates of the bacteria. The adsorption of as-synthesized AgNPs on orthodontic wires imparts strong antibacterial attributes to the Ni-Ti orthodontic wires. We speculate that AgNP-impregnated orthodontic wires acquire an intrinsic potential to inhibit bacterial growth upon their use in clinical settings.

DATA AVAILABILITY STATEMENT

The original contributions presented in the study are included in the article/**Supplementary Material**; further inquiries can be directed to the corresponding authors.

AUTHOR CONTRIBUTIONS

MO conceived the concept. SK and SS designed the experiments. SF, NK, AO MU, AA, IW, and FJ performed the experiments. SF, MK, IA, and NK analyzed the data. MO and SK contributed the reagents/materials/analysis tools.

ACKNOWLEDGMENTS

The authors express their gratitude to the coordinator, Interdisciplinary Biotechnology Unit, Aligarh Muslim University, Aligarh, for providing facilities to complete this study.

SUPPLEMENTARY MATERIAL

The Supplementary Material for this article can be found online at: <https://www.frontiersin.org/articles/10.3389/fnano.2022.780783/full#supplementary-material>

REFERENCES

- Abbasi, E., Milani, M., Fekri Aval, S., Kouhi, M., Akbarzadeh, A., Tayefi Nasrabadi, H., et al. (2016). Silver Nanoparticles: Synthesis Methods, Bio-Applications and Properties. *Crit. Rev. Microbiol.* 42 (2), 173–180. doi:10.3109/1040841X.2014.912200
- Bhosale, R. R., Kulkarni, A. S., Gilda, S. S., Aloorkar, N. H., Osmani, R. A., and Harkare, B. R. (2014). Innovative Eco-Friendly Approaches for green Synthesis of Silver Nanoparticles. *PCI- Approved-IJPSN* 7 (1), 2328–2337. doi:10.37285/ijpsn.2014.7.1.3
- D'Agostino, A., Taglietti, A., Grisoli, P., Dacarro, G., Cucca, L., Patrini, M., et al. (2016). Seed Mediated Growth of Silver Nanoplates on Glass: Exploiting the Bimodal Antibacterial Effect by Near IR Photo-thermal Action and Ag+ Release. *RSC Adv.* 6 (74), 70414–70423. doi:10.1039/c6ra11608f

- Decker, E. M., Dietrich, I., Klein, C., and von Ohle, C. (2011). Dynamic Production of Soluble Extracellular Polysaccharides by Streptococcus Mutans. *Int. J. Dent* 2011, 435830. doi:10.1155/2011/435830
- dos Santos, M. A., Paterno, L. G., Moreira, S. G., and Sales, M. J. (2019). Original Photochemical Synthesis of Ag Nanoparticles Mediated by Potato Starch. *SN Appl. Sci.* 1 (6), 1–3. doi:10.1007/s42452-019-0586-1
- Dutta, D., Sahoo, A. K., Chattopadhyay, A., and Ghosh, S. S. (2016). Bimetallic Silver Nanoparticle-Gold Nanocluster Embedded Composite Nanoparticles for Cancer Theranostics. *J. Mater. Chem. B* 4 (4), 793–800. doi:10.1039/c5tb01583a
- Farkas, K., Varsani, A., and Pang, L. (2015). Adsorption of Rotavirus, MS2 Bacteriophage and Surface-Modified Silica Nanoparticles to Hydrophobic Matter. *Food Environ. Virol.* 7 (3), 261–268. doi:10.1007/s12560-014-9171-3
- Francolini, I., Vuotto, C., Piozzi, A., and Donelli, G. (2017). Antifouling and Antimicrobial Biomaterials: an Overview. *Apmis* 125 (4), 392–417. doi:10.1111/apm.12675

- Gallardo, C. M. C., Hernandez, S. A. C., Lopez, L. F. M., and Rojas, J. P. G. (2019). *Universidad de Chile Preparation process of dental and orthopedic acrylic materials with antimicrobial properties using copper nanoparticle technology*. U.S. Patent Application 16/067,053.
- Guerrero-Martínez, A., Pérez-Juste, J., and Liz-Marzán, L. M. (2010). Recent Progress on Silica Coating of Nanoparticles and Related Nanomaterials. *Adv. Mater.* 22 (11), 1182–1195. doi:10.1002/adma.200901263
- Hu, J., Lin, J., Zhang, Y., Lin, Z., Qiao, Z., Liu, Z., et al. (2019). A New Anti-biofilm Strategy of Enabling Arbitrary Surfaces of Materials and Devices with Robust Bacterial Anti-adhesion via a Spraying Modified Microsphere Method. *J. Mater. Chem. A* 7 (45), 26039–26052. doi:10.1039/c9ta07236e
- Iravani, S., Korbekandi, H., Mirmohammadi, S. V., and Zolfaghari, B. (2014). Synthesis of Silver Nanoparticles: Chemical, Physical and Biological Methods. *Res. Pharm. Sci.* 9 (6), 385–406.
- Khan, I., Saeed, K., and Khan, I. (2019). Nanoparticles: Properties, Applications and Toxicities. *Arabian J. Chem.* 12 (7), 908–931. doi:10.1016/j.arabjc.2017.05.011
- Koo, H., Allan, R. N., Howlin, R. P., Stoodley, P., and Hall-Stoodley, L. (2017). Targeting Microbial Biofilms: Current and Prospective Therapeutic Strategies. *Nat. Rev. Microbiol.* 15 (12), 740–755. PMID: 28944770; PMCID: PMC5685531. doi:10.1038/nrmicro.2017.99
- Lekhadia, D. R. (2018). “Nanotechnology in Orthodontics-Futuristic Approach,” in *Dental Applications of Nanotechnology* (Cham: Springer), 155–175. doi:10.1007/978-3-319-97634-1_9
- Li, Y., Zhang, W., Niu, J., and Chen, Y. (2013). Surface-coating-dependent Dissolution, Aggregation, and Reactive Oxygen Species (ROS) Generation of Silver Nanoparticles under Different Irradiation Conditions. *Environ. Sci. Technol.* 47 (18), 10293–10301. doi:10.1021/es400945v
- Lim, T. K. (2014). “Hibiscus Rosa-Sinensis,” in *Edible Medicinal and Non Medicinal Plants* (Dordrecht: Springer), 306–323. doi:10.1007/978-94-017-8748-2_22
- Loo, Y. Y., Chieng, B. W., Nishibuchi, M., and Radu, S. (2012). Synthesis of Silver Nanoparticles by Using tea Leaf Extract from Camellia Sinensis. *Int. J. Nanomedicine* 7, 4263–4267. doi:10.2147/IJN.S33344
- Mohanty, S., Mishra, S., Jena, P., Jacob, B., Sarkar, B., and Sonawane, A. (2012). An Investigation on the Antibacterial, Cytotoxic, and Antibiofilm Efficacy of Starch-Stabilized Silver Nanoparticles. *Nanomedicine: Nanotechnology, Biol. Med.* 8 (6), 916–924. doi:10.1016/j.nano.2011.11.007
- Montgomery, C. P., Daniels, M., Zhao, F., Alegre, M.-L., Chong, A. S., and Daum, R. S. (2014). Protective Immunity against Recurrent *Staphylococcus aureus* Skin Infection Requires Antibody and interleukin-17A. *Infect. Immun.* 82 (5), 2125–2134. Epub 2014 Mar 10. PMID: 24614654; PMCID: PMC3993461. doi:10.1128/IAI.01491-14
- Mourdikoudis, S., Pallares, R. M., and Thanh, N. T. K. (2018). Characterization Techniques for Nanoparticles: Comparison and Complementarity upon Studying Nanoparticle Properties. *Nanoscale* 10 (27), 12871–12934. doi:10.1039/c8nr02278j
- Petros, R. A., and DeSimone, J. M. (2010). Strategies in the Design of Nanoparticles for Therapeutic Applications. *Nat. Rev. Drug Discov.* 9 (8), 615–627. doi:10.1038/nrd2591
- Ramasamy, M., and Lee, J. (2016). Recent Nanotechnology Approaches for Prevention and Treatment of Biofilm-Associated Infections on Medical Devices. *Biomed. Res. Int.* 2016, 1851242. doi:10.1155/2016/1851242
- Ramya, M., and Subapriya, M. S. (2012). Green Synthesis of Silver Nanoparticles. *Int. J. Pharm. Med. Biol. Sci.* 1 (1), 54–61.
- Ritter, A. V., Eidson, R. S., and Donovan, T. E. (2014). *Dental Caries: Etiology, Clinical Characteristics, Risk Assessment, and Management*. Missouri, TX: Sturdevant's Art & Science of Operative Dentistry-E-Book, 41.
- Rizzello, L., and Pompa, P. P. (2014). Nanosilver-based Antibacterial Drugs and Devices: Mechanisms, Methodological Drawbacks, and Guidelines. *Chem. Soc. Rev.* 43 (5), 1501–1518. doi:10.1039/c3cs60218d
- Shewale, P., Hiray, Y., and Patil, R. (2012). Antidepressant-like Activity of Anthocyanidins from Hibiscus Rosa-Sinensis Flowers in Tail Suspension Test and Forced Swim Test. *Indian J. Pharmacol.* 44 (4), 454. doi:10.4103/0253-7613.99303
- Sun, Q., Cai, X., Li, J., Zheng, M., Chen, Z., and Yu, C.-P. (2014). Green Synthesis of Silver Nanoparticles Using tea Leaf Extract and Evaluation of Their Stability and Antibacterial Activity. *Colloids Surf. A: Physicochemical Eng. Aspects* 444, 226–231. doi:10.1016/j.colsurfa.2013.12.065
- Vashist, A., Vashist, A., Gupta, Y. K., and Ahmad, S. (2014). Recent Advances in Hydrogel Based Drug Delivery Systems for the Human Body. *J. Mater. Chem. B* 2 (2), 147–166. doi:10.1039/c3tb21016b
- Wang, L., Hu, C., and Shao, L. (2017). The Antimicrobial Activity of Nanoparticles: Present Situation and Prospects for the Future. *Ijn* 12, 1227–1249. doi:10.2147/ijn.s121956
- Wang, Y., Jayan, G., Patwardhan, D., and Phillips, K. S. (2017). “Antimicrobial and Anti-biofilm Medical Devices: Public Health and Regulatory Science Challenges,” in *Antimicrobial Coatings and Modifications on Medical Devices 2017* (Cham: Springer), 37–65.

Conflict of Interest: The authors declare that the research was conducted in the absence of any commercial or financial relationships that could be construed as a potential conflict of interest.

Publisher's Note: All claims expressed in this article are solely those of the authors and do not necessarily represent those of their affiliated organizations, or those of the publisher, the editors, and the reviewers. Any product that may be evaluated in this article, or claim that may be made by its manufacturer, is not guaranteed or endorsed by the publisher.

Copyright © 2022 Farheen, Oanz, Khan, Umar, Jamal, Altaf, Kashif, Alshameri, Somavarapu, Wani, Khan and Owais. This is an open-access article distributed under the terms of the Creative Commons Attribution License (CC BY). The use, distribution or reproduction in other forums is permitted, provided the original author(s) and the copyright owner(s) are credited and that the original publication in this journal is cited, in accordance with accepted academic practice. No use, distribution or reproduction is permitted which does not comply with these terms.